A novel discretization scheme and computational method to handle high contrast in computational electromagnetic problems

Zhifeng Sheng
z.sheng@ewi.tudelft.nl

Abstract

This paper presents the application of the least-squares field integrated method based on hybrid linear finite elements in time-domain electromagnetic (EM) problems with high contrast interfaces. The method proposes the use of edge based linear finite elements over nodal elements and edge elements of Whitney form. It shows how the equations have to be accommodated to yield a correct solution. It proposes a general strategy to combine edge linear finite elements and nodal linear finite elements. The resulting algorithms are stable and achieve high quality field interpolation even in the presence of very high contrasts. The performance and stability of the new method is shown by exhibiting the time-domain solution of a high contrast EM problem for which an analytic solution is known. Unaxial Perfectly Matched Layers are used to truncate the computational domain with absorbing boundary when needed.

I. Introduction

In strongly heterogeneous media, the constitutive parameters can jump by large amounts upon crossing the material interfaces. On a global scale, the EM field components are, therefore, not differentiable and Maxwell's equations in differential form cannot be used: one has to resort to the original integral form of the EM field relations as the basis for the computational method. The appropriate integral form is provided by the classical interrelations between the curl of the electric/magnetic field strength along a closed curve and the time rate of change of the magnetic/electric flux passing through a surface with the circulation loop as boundary. For these to hold, only integrability of the field is needed, which condition we impose in accordance with the physical condition of boundedness of the field quantities. To satisfy the constitutive relations (that are representative of physical volume effects), a fitting continuation of the boundary representations of the field components of an element into its interior is needed. We construct a consistent algorithm that meets all of these requirements, using a simplicial geometrical discretization combined with piecewise linear representation of the electric and magnetic field components along the edges of the elements, piecewise linear extrapolations into the interior of the elements and taking constant values of the constitutive coefficients in these interiors. We also use piecewise linear representations. Furthermore, we use NETGEN[13] to discretize the computational domain with a 2D(triangular)/3D(tetrahedron) mesh. We use simple boundary conditions (PEC, PMC) to truncate the computational domain. After properly assembling the local matrices, we obtain a symmetric positive definite system of algebraic equations, which we solve with a preconditioned iterative method. We test the accuracy of the method by implementing the four domain problem treated analytically in [8] in the time domain using our method. This experiment also documents the stability of our approach, we can provide theoretical proof as well.

II. Mesh generation

In a finite element package, geometrical discretization is done by a mesh generator. With a non-uniform mesh, we have good control over the coarseness of the mesh. In particular, the mesh should be refined where more local features reside, so that the numerical error can be minimized; meanwhile, the mesh should be coarser where the change in configuration is smooth. It also has been shown that equilateral triangles are the best shapes of finite elements. Any triangle that is close to being equilateral introduces small numerical dispersion. We use NETGEN[13] to generate 2D/3D mesh. A triangle finite element is identified with three vertexes delimiting it. It is advantageous to number the vertexes in such a way that the face vectors of the all the simplexes point to the same direction (either the positive z direction or the negative z direction, here we choose the positive z direction.). This implies that the vertexes delimiting an element should be numbered counterclockwise.

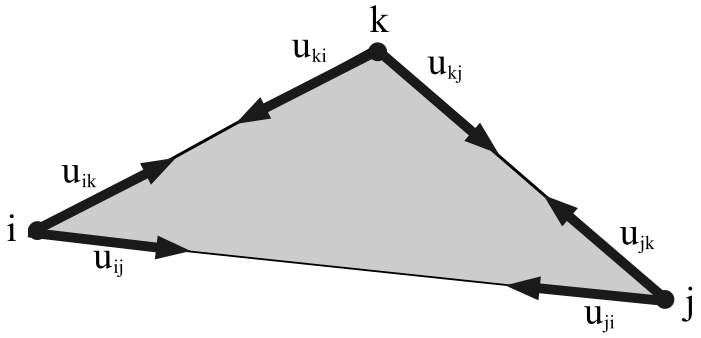

Fig. 1. Degrees of freedom on an two dimensional consistently linear finite element

III. Finite elements

Due to the interface conditions, a straight-forward application of the linear expansion function would lead to large numerical error or excessive mesh refinement. Applying these interfaces conditions as constraints would result in semi-positive definite system matrices which are difficult to solve (see [12], [3]). It is advantageous to take them into account when discretizing the field quantities. The key point in the discretization technique is to approximate the field quantities, which are known to be continuous, with nodal linear finite element, and the discontinuous ones are approximated with edge based finite elements.

A. Geometrical quantities

Before introducing the expansion functions (shape functions) of linear finite elements, we shall define a few geometrical quantities (see Fig. 1). Let $\Delta(r_i, r_j, r_k)$ or $\Delta(i, j, k)$ be the triangle delimited by three vertexes with coordinates r_i, r_j, r_k; $|\Delta(i, j, k)|$ be the area in triangle $\Delta(i, j, k)$; r_i be the spatial coordinate of the vertex i; $e_{ij} = \frac{r_j - r_i}{|r_j - r_i|}$ be the unit vector pointing from vertex i to j; $a_k = i_z \times e_{ij}$ be the normal unit vector perpendicular to the edge delimited by vertex i and j; $\phi_i(r) = \frac{|\Delta(r, r_j, r_k)|}{|\Delta(r_i, r_j, r_k)|}, \forall r \in \Delta(r_i, r_j, r_k)$ be the linear shape function. By definition, $\phi_i(r)$ is equal to 1 on vertex i and 0 on other vertexes in $\Delta(r_i, r_j, r_k)$.

B. Nodal linear finite element

In a homogeneous sub-domain, the field quantities v are continuous; to preserve this continuity, the field quantity should be approximated with nodal linear finite element. The linear expansion function can be used to construct the local linear interpolation $\mathbf{v}$ of v in $\Delta(r_i, r_j, r_k)$.

$$\mathbf{v}(r) = \sum_{l \in (i,j,k)} v(l)\phi_l(r) \tag{1}$$

Both the tangential component and normal component of $\mathbf{v}$ are continuous across the interface. For quantities belonging to $\mathcal{H}^1(\Omega) = \{v \in L^2(\Omega); v' \in L^2(\Omega)\}$. It has the approximation error of the order $O(h^2)$ (where h denotes the mesh size).

C. Edge based consistently linear finite elements

To keep the tangential components of the field quantities u (u is a vectorial quantity) continuous across the interfaces, we shall only use the well defined continuous components (u_{lh} where $l, h \in (i, j, k), l \neq h$, see Fig. 1) on vertexes to construct a linear interpolation over any triangle $\Delta(i, j, k)$. $u(i)$ specifies the two dimensional field quantity on vertex i. The quantity u on a node of a finite element can be fully expressed in terms of the tangential components on the incident edges:

$$u(i) = u_{ij}\frac{a_j}{e_{ij} \cdot a_j} + u_{ik}\frac{a_k}{e_{ik} \cdot a_k} = \sum_{l \in (i,j,k), l \neq i} u_{il}\frac{a_l}{e_{il} \cdot a_l} \tag{2}$$

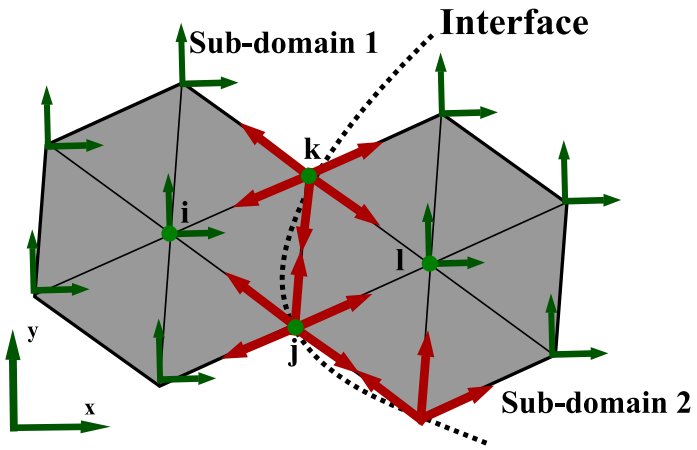

Fig. 2. The allocation of the nodal- and edge- linear finite elements.

With u defined on each vertex, the linear shape function $\phi_l(r)$ can be used to construct the local linear interpolation $\mathbf{u}(r)$ of $u(r), r \in \Delta(i,j,k)$, as follows:

$$\mathbf{u}(r) = \sum_{l\in(i,j,k)} u(l)\phi_l(r) = \sum_{l\in(i,j,k)} \sum_{h\in(i,j,k),h\neq l} u_{lh}\frac{a_h}{e_{lh}\cdot a_h}\phi_l(r) \tag{3}$$

unlike the Whitney-1 elements, the edge based consistently linear finite element does not satisfy the divergence free property; therefore we need to enforce the divergence free condition explicitly. On the other hand, for quantities belonging to $\mathcal{H}(curl;\Omega) = \{v \in [L^2(\Omega)]^{n_d} : \nabla \times v \in [L^2(\Omega)]^{n_d}\}$, the consistently linear expansion has the local approximation error of the order $O(h^2)$ instead of $O(h)$ for Whitney edge elements. The consistently linear expansion function was used first by Gerrit Mur in [6].

D. Combination of node- and edge- finite element expansion

To preserve the continuity properties of field quantities without introducing too many unnecessary unknowns, we use edge based consistently linear finite elements only on material interfaces, node linear finite elements in homogeneous subdomains (see Fig. 2). Hereinafter, we refer to this combination as hybrid linear finite elements.

IV. Two dimensional magnetostatic problem

To study the merits of hybrid finite element and its convergent rate, we shall take a simple two dimensional magnetostatic problem with analytic solutions.

A. The magnetostatic equations

In the computation domain Ω with its boundary $\partial\Omega$, given an arbitrary surface S with its boundary ∂S, The equations to be solved in magnetostatic problem are list as follows:

$$\oint_{\partial S} H \cdot dl = \int_S J \cdot ds \tag{4}$$

$$\oint_S B \cdot ds = 0 \tag{5}$$

and interface condition

$$[n \cdot B] = 0 \text{ on } \Gamma_i \tag{6}$$

$$[n \times H] = 0 \text{ on } \Gamma_i \tag{7}$$

$[A] = \lim A(\Gamma^+) - \lim A(\Gamma^-)$ denotes the jump of a quantity A across the material interface Γ. n is a unit vector normal to the interface. Finally, the constitutive relation

$$B = \mu_r \mu_0 H \tag{8}$$

B. The (weighted) least-squares functional

With appropriate edge/hybrid finite elements to approximate magnetic field strength H, the interface condition Eq. (7) is satisfied in the whole computational domain; therefore we don't have to consider that equation in the least-squares formulation. Let N be the number of finite elements in the computational domain; each finite element have n faces (two-dimensional triangle elements are extended as prism elements with infinite height. Prism element has 4 faces. $S_j, 1 \leq j \leq 4$); the jth face of ith finite element be donated as S_{ij} with its boundary defined as ∂S_{ij}, over the computational domain Ω , the least-squares functional is defined as:

$$\begin{aligned} I &: \mathcal{H}(curl) \rightarrow R, \\ I(H) &= \sum_{i=1}^{N}\{\sum_{j=1}^{n} a_1(ij)\| \oint_{\partial S_{ij}} H \cdot dl - \int_{S_{ij}} J \cdot ds\|^2 + a_2(ij)\| \oint_{\cup_{j=1}^{n} S_{ij}} (\mu H \cdot n)\, ds\|^2\} \\ &+ \sum_{\text{for all } \Gamma_i} \|[(n \cdot \mu H)]\|^2 \end{aligned} \tag{9}$$

for which the exact solution is the minimizer. $a_1(ij)$, $a_2(ij)$ are positive weighting factors. With appropriate boundary conditions (eg. PEC, PMC) implemented either implicitly by adding the corresponding squared terms into the least-squares functional or explicitly by restricting the shape functions to satisfy the boundary conditions, the magnetic field strengths can be solved by finding the minimizer to the least-squares functional $I(H)$; On the other hand, the least-squares functional $I(H)$ serves as a nature indicator for finite element refinement.

C. A test problem

Let us consider two dimensional domain $\Omega = \{0 \leq x \leq 1, 0 \leq y \leq 1\}$, and J is chosen such that the exact magnetic field strength is:

$$H_{xy} = \frac{\pi \sin \pi x \, \cos \pi y}{\mu}\, i_x - \frac{\pi \cos \pi x \, \sin \pi y}{\mu}\, i_y \tag{10}$$

the electric current in the domain is:

$$J = \frac{2\pi^2 \, \sin \pi x \, \sin \pi y}{\mu}\, i_z \tag{11}$$

The chosen material configuration is:

$$\mu_r = \begin{cases} 1000 & \text{if } 0 \leq x \leq 0.5, 0 \leq y \leq 0.5 \\ 1 \end{cases} \tag{12}$$

The above analytic solution satisfies the magnetostatic equations with PEC boundary condition.

D. Numerical result

With the same interface conforming mesh and the same least-squares functional, we compute the magnetic field strengths in domain Ω with hybrid linear finite elements, nodal linear finite elements and edge linear finite elements. The linear system of equations is solved with preconditioned iterative method (see Section VI-J2). The computed field strengths are sampled and plotted on the same points of the domain D. Note that, In Fig. 3, the solutions of the edge based finite element method and hybrid finite element method display correctly the singularity in the left-bottom sub-domain; on the contrary, the solution of the node based linear finite element least-squares method tends to be incorrect in the singular region. Similar result is observed in [4]. To study the rate of convergence of these least-squares finite element methods, we choose to experiment this method with the test problem and the a homogeneous material configuration ($\mu_r = 1$). The relative mean square error is plotted in Fig. 4. It is obvious from Fig. 4(a) that the edge element LSFEM and its hybrid version have the same convergence rate as the node based linear finite element method; From Fig. 4(b), it can be seen that the node based LSFEM converges to a spurious solution in the case of high contrast.

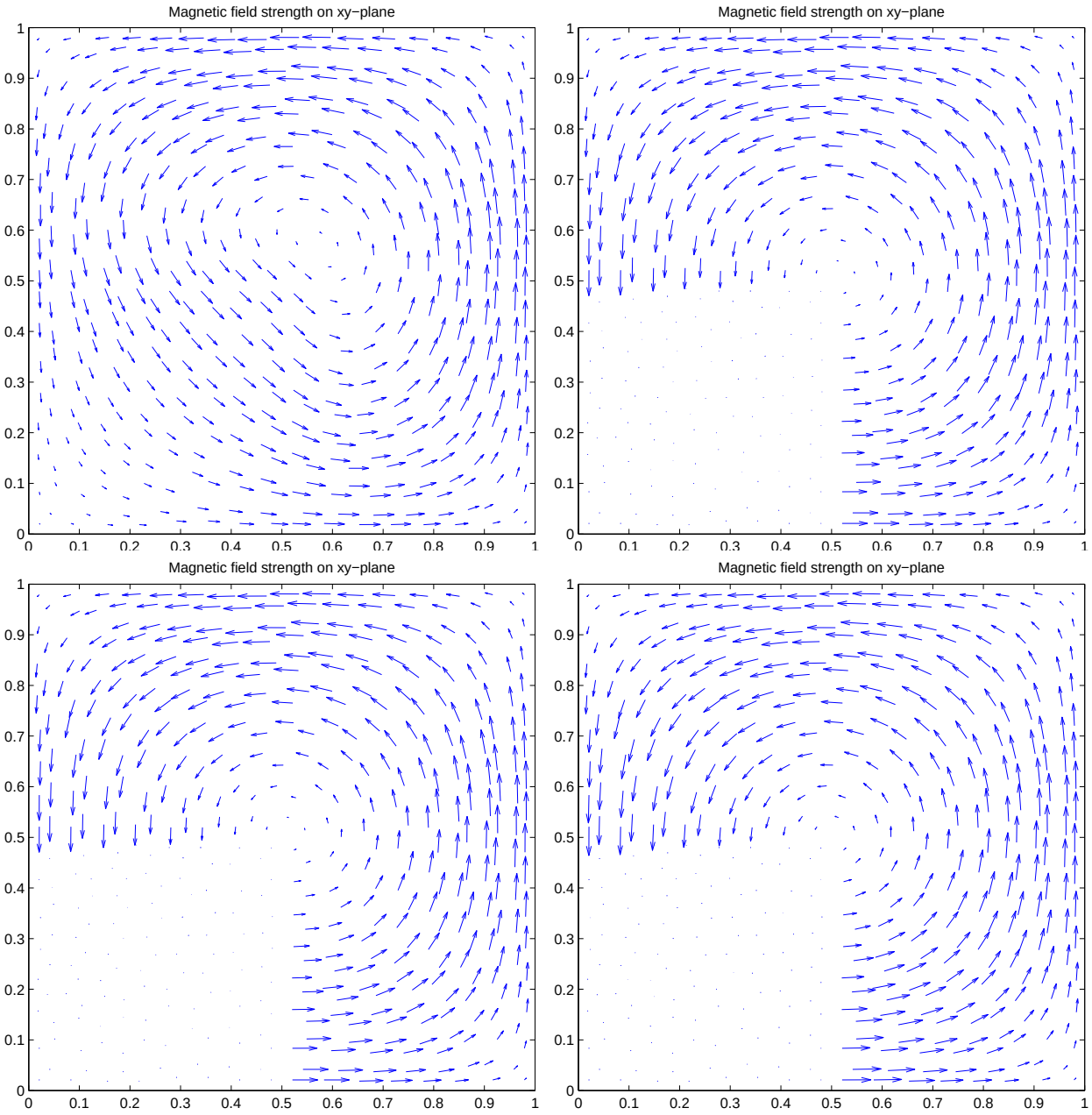

Fig. 3. Magnetic field strengths of the test problem, the solution of nodal linear finite elements based method (a), the solution of hybrid linear finite elements based method(b), the solution of edge linear finite elements based method (c), the analytic solution (d)

V. Domain integrated Field equations

In the computation domain Ω with its boundary $\partial\Omega$, given a (sufficiently smooth and small) surface S with boundary ∂S, Maxwell's equations in the surface integrated form are

$$\oint_{\partial S} H \cdot dl = \int_S \{\partial_t D + \sigma^e E + J^{imp}\} \cdot ds \tag{13}$$

$$\oint_{\partial S} E \cdot dl = -\int_S \{\partial_t B + \sigma^m H + K^{imp}\} \cdot ds \tag{14}$$

Let $J^{tot} = \partial_t B + \sigma^m H + K^{imp}$, $K^{tot} = \partial_t D + \sigma^e E + J^{imp}$ The compatibility relations on a volume V with its closed surface ∂V in their integrated form are:

$$\oint_{\partial V} J^{tot} \cdot ds = 0 \tag{15}$$

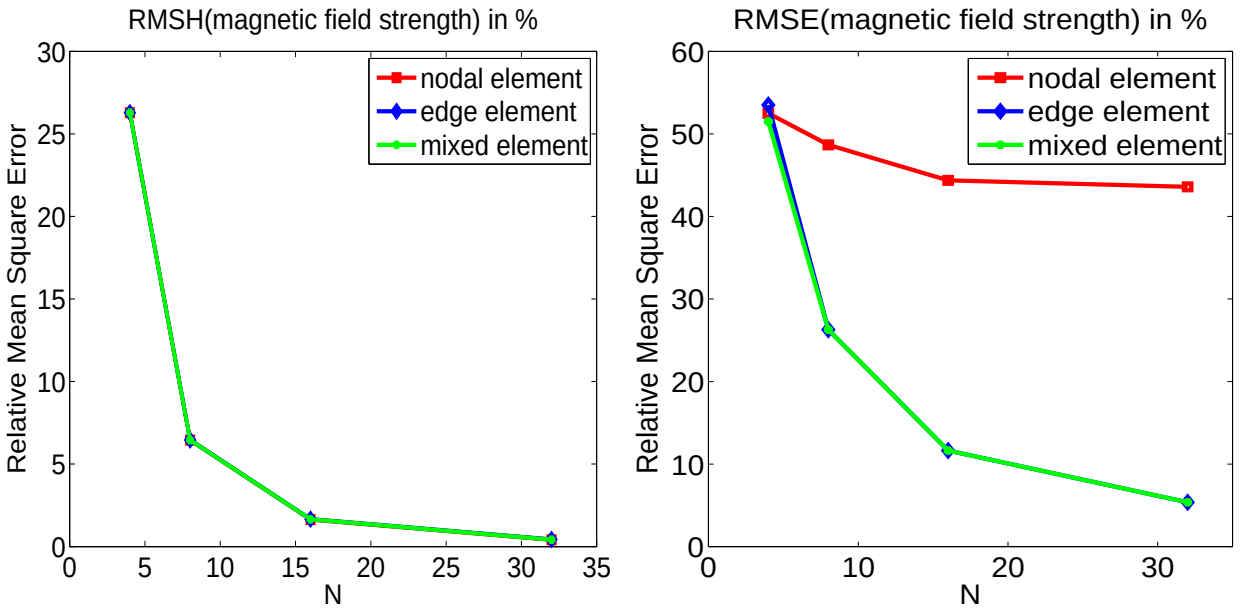

Fig. 4. The relative mean square error of numerical solutions in homogeneous domain(a), The relative mean square error of numerical solutions in test configuration with high contrast (b). N is the number of finite element used in one dimension

$$\oint_{\partial V} K^{tot} \cdot ds = 0 \tag{16}$$

Computational domain is truncated by PEC and PMC boundary conditions:

$$n \times E = 0 \text{ on } \partial\Omega_1 \quad n \cdot K^{tot} = 0 \text{ on } \partial\Omega_1 \text{ (PEC boundary)}$$
$$n \times H = 0 \text{ on } \partial\Omega_2 \quad n \cdot J^{tot} = 0 \text{ on } \partial\Omega_2 \text{ (PMC boundary)}$$

where $\partial\Omega_1 \cap \partial\Omega_2 = \phi$, $\partial\Omega_1 \cup \partial\Omega_2 = \partial\Omega$; $\varepsilon(x_r)$ is the permittivity, $\mu(x_r)$ the permeability. $\sigma^e(x_r)$ the electric conductivity, $\sigma^m(x_r)$ the magnetic conductivity. Last but not the least, the interface conditions are:

$$[n \cdot K^{tot}] = 0 \text{ on } \Gamma_i \quad [n \times H] = 0 \text{ on } \Gamma_i$$
$$[n \cdot J^{tot}] = 0 \text{ on } \Gamma_i \quad [n \times E] = 0 \text{ on } \Gamma_i$$

where $[A] = \lim A(\Gamma^+) - \lim A(\Gamma^-)$ denotes the jump of a quantity A across the material interface Γ. The constitutive relations are:

$$D(x_r, t) = \varepsilon(x_r)E(x_r, t) \quad B(x_r, t) = \mu(x_r)H(x_r, t)$$

VI. Two dimensional electromagnetic problem: the perpendicular polarization case

In this section, we show how to utilize the hybrid linear finite elements to solve 2D electromagnetic problems.

A. Two-dimensional electromagnetic problems and spatial- temporal- discretization

The 2D problem is characterized by invariance in the z direction. And we consider perpendicular polarized field only. In this case, the electric field strength is interpolated with nodal linear finite elements, since this field is always tangential to the material interfaces. The magnetic field strength, however, is approximated by hybrid linear finite elements as mentioned in Section III-D. This means that the magnetic field strength is interpolated by edge based linear finite element at the material interfaces and by nodal linear finite element in homogeneous sub-domains. Our discretization procedure is similar to that in [9], except that the discretized Maxwell's equations are derived there for static problems, while we work with the full Maxwell system in the time-domain. To implement a time stepping scheme for the spatially discretized Maxwell's equations, we introduce the time instance $t_i = i\delta t$, where $\delta t > 0$ is the time step, and integrate Maxwell's equations from $t = t_{i-1}$ to $t = t_i$. All integrals that can not be computed analytically are discretized using the trapezoidal rule. To maintain accuracy in the time-domain and avoid computing too many unnecessary time-steps, we choose the time-step δt corresponding to a CFL number between 1 and 2 for the smallest element (see [7]).

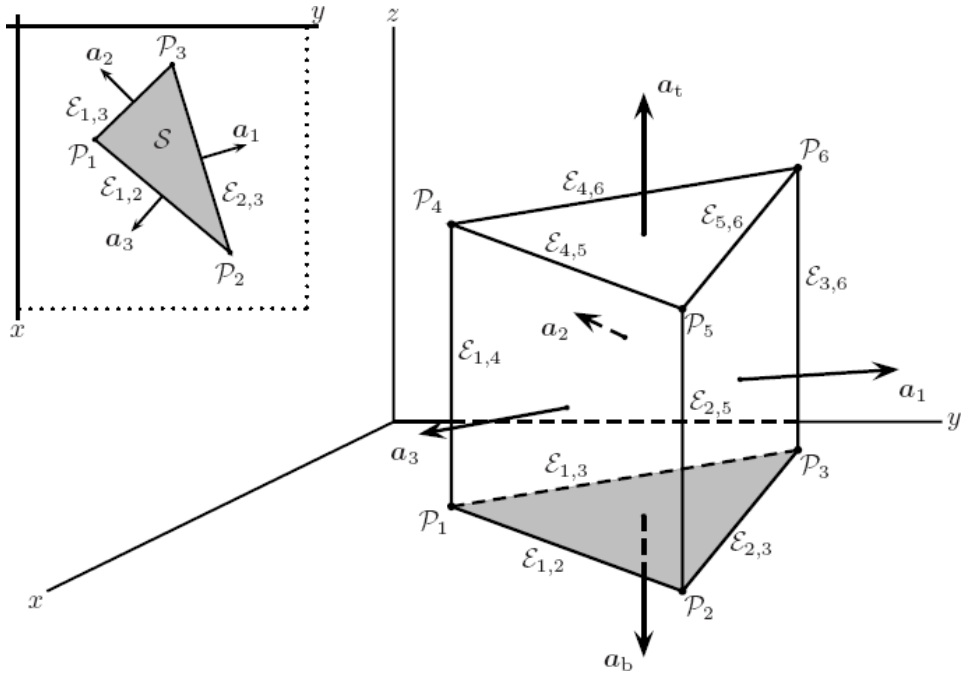

Fig. 5. The prism element.

B. Normalization

Before formulating the system of equations, it is important to normalize these system equations so that the system has better spectral properties. Let L be a problem related reference length, we normalize the spatial coordinate, time coordinate, field quantities, EM sources and matter parameters as:

$$\widehat{x} = \frac{x}{L} \;\; \widehat{t} = \frac{c_0 t}{L} \;\; \widehat{E}(\widehat{x},\widehat{t}) = E(L\widehat{x}, \frac{L\widehat{t}}{c_0})$$
$$\widehat{H}(\widehat{x},\widehat{t}) = \sqrt{\frac{\mu_0}{\varepsilon_0}} H(L\widehat{x}, \frac{L\widehat{t}}{c_0}) \;\; \widehat{J}^{imp}(\widehat{x},\widehat{t}) = L\sqrt{\frac{\mu_0}{\varepsilon_0}} J^{imp}(L\widehat{x}, \frac{L\widehat{t}}{c_0})$$
$$K^{imp}(\widehat{x},\widehat{t}) = LK^{imp}(L\widehat{x}, \frac{L\widehat{t}}{c_0}) \;\; \widehat{\sigma}^e(\widehat{x}) = L\sqrt{\frac{\mu_0}{\varepsilon_0}}\sigma^e(L\widehat{x})$$
$$\widehat{\sigma}^m(\widehat{x}) = L\sqrt{\frac{\varepsilon_0}{\mu_0}}\sigma^m(L\widehat{x}) \;\; \widehat{\varepsilon}(\widehat{x}) = \varepsilon(L\widehat{x}) \;\; \widehat{\mu}(\widehat{x}) = \mu(L\widehat{x})$$

We implement the least-squares field integrated method with normalized Maxwell's equations.

C. Discrete Surface Integrated Field Equations

Detailed derivation is given in Jorna's thesis, here we give a short survey on these equations. Applying the equation 13 on the face delimited by points $i = P_1, j = P_2, k = P_3$ see Fig.5, and make use of the linear expansions. We get:

$$\begin{aligned}\frac{1}{2}l_i[H_k(t)\cdot e_{kj} + H_j(t)\cdot e_{kj}] + \frac{1}{2}l_j[H_i(t)\cdot e_{ik} + H_k(t)\cdot e_{ik}] + \frac{1}{2}l_k[H_j(t)\cdot e_{ji} + H_i(t)\cdot e_{ji}] \\ + \frac{A}{3}[(\sigma^e_{izz} + \varepsilon_{izz}\partial_t)E_{iz}(t) + (\sigma^e_{jzz} + \varepsilon_{jzz}\partial_t)E_{jz}(t) + (\sigma^e_{kzz} + \varepsilon_{kzz}\partial_t)E_{kz}(t)] \\ = -\frac{A}{3}[J^{imp}_{iz}(t) + J^{imp}_{jz}(t) + J^{imp}_{kz}(t)] \qquad (17)\end{aligned}$$

Where $H_l(t),\ l \in \{i,j,k\}$ may be represented by either nodal linear expansion (Eq. 1) or edge linear expansion (Eq. 2). Apply the equation 14 on the face delimited by points $j = P_2, k = P_3, k' = P_6, j' = P_5$, and make use

of the linear expansions. We get:

$$E_{kz} - E_{jz} = -\frac{1}{2} l_i [K_k^{tot} \cdot a_i + K_j^{tot} \cdot a_i] \tag{18}$$

Apply the equation 14 on the face delimited by points $i = P_1, k = P_3, k' = P_6, i' = P_4$ and use the linear approximation. We get:

$$E_{iz} - E_{kz} = -\frac{1}{2} l_j [K_i^{tot} \cdot a_j + K_k^{tot} \cdot a_j] \tag{19}$$

Apply the equation 14 on the face delimited by points $j = P_3, i = P_2, i' = P_4, j' = P_5$ and use the linear approximation. We get:

$$E_{jz} - E_{iz} = -\frac{1}{2} l_k [K_j^{tot} \cdot a_k + K_i^{tot} \cdot a_k] \tag{20}$$

D. Constitutive Relations

To determine the electromagnetic field strength, the constitutive relations are described via equations

$$K^{tot}(t) = \sigma^m H(t) + \mu \partial_t H(t) + K^{imp}(t) \tag{21}$$

assume the magnetic constitutive parameters are isotropic with respect to x and y direction, we have, for edge expansions:

$$K_i^{tot}(t) - (\sigma_i^m + \mu_i \partial_t)[H_{ij}(t)\frac{a_j}{e_{ij}a_j} + H_{ik}(t)\frac{a_k}{e_{ik}a_k}] = K_i^{imp}(t), \quad i \neq j \neq k; \quad i,j,k \in \{P_1, P_2, P_3\} \tag{22}$$

and for nodal element:

$$K_i^{tot}(t) - (\sigma_i^m + \mu_i \partial_t) H_i(t) = K_i^{imp}(t), \quad i \in \{P_1, P_2, P_3\} \tag{23}$$

To simplify the system to be solved, we substitute the consititutive relations into equations (18-20) and eliminate unknown $K_i^{tot}(t)$.

E. Discrete system

The discrete surface integrated equations should be then temporally discretized with the trapezium rule. All these discrete equations together form a system of linear equations to be solved.

1) Discrete local system of linear equations: For a triangular finite element, the set of local (over-determined) discrete integrated field system is (Note that: in this equation, we make no distinguish between the local matrices associated with nodal finite elements and those associated with edge finite elements. As in the remaining of this paper, the difference will be clear) :

$$(C^e + \frac{\Delta t}{2} L^e + \frac{\Delta t}{2} K^e) \begin{bmatrix} H^e(n+1) \\ E^e(n+1) \end{bmatrix} = (C^e - \frac{\Delta t}{2} L^e - \frac{\Delta t}{2} K^e) \begin{bmatrix} H^e(n) \\ E^e(n) \end{bmatrix} + \frac{\Delta t}{2} F^e (\begin{bmatrix} K^e(n+1) \\ J^e(n+1) \end{bmatrix} + \begin{bmatrix} K^e(n) \\ J^e(n) \end{bmatrix})$$

$$K^e = \begin{bmatrix} 0 & D_e^e \\ -D_h^e & 0 \end{bmatrix}, C^e = \begin{bmatrix} M_\mu^e & 0 \\ 0 & M_\varepsilon^e \end{bmatrix}, L^e = \begin{bmatrix} M_{\sigma^m}^e & 0 \\ 0 & M_{\sigma^e}^e \end{bmatrix}, F^e = \begin{bmatrix} F_K^e & 0 \\ 0 & F_J^e \end{bmatrix}$$

Note that: the matrices with superscript ^{e} are local matrices, and the ones without superscript ^{e} are global matrices. If the media is loss-less, then $L^e = 0$ and $L = 0$. The local matrices are different for nodal finite element and edge-finite element. For the nodal finite element $\Delta(1,2,3)$ (where the vertexes are numbered locally and $1, 2, 3$ denote

the local numbering of the vertexes. Let A be the area of $\Delta(1,2,3)$.), the local matrices for nodal finite element and the corresponding discrete interface condition matrix are defined as follows:

$$
\begin{aligned}
X^e &= \begin{bmatrix} X_1^e & 0 \\ 0 & X_2^e \end{bmatrix}, X_1^e = \begin{bmatrix} \frac{\sigma_1^m}{\mu_1} & 0 & 0 & 0 & 0 & 0 \\ 0 & \frac{\sigma_1^m}{\mu_1} & 0 & 0 & 0 & 0 \\ 0 & 0 & \frac{\sigma_2^m}{\mu_2} & 0 & 0 & 0 \\ 0 & 0 & 0 & \frac{\sigma_2^m}{\mu_2} & 0 & 0 \\ 0 & 0 & 0 & 0 & \frac{\sigma_3^m}{\mu_3} & 0 \\ 0 & 0 & 0 & 0 & 0 & \frac{\sigma_3^m}{\mu_3} \end{bmatrix}, X_2^e = \begin{bmatrix} \frac{\sigma_1^e}{\varepsilon_1} & 0 & 0 \\ 0 & \frac{\sigma_2^e}{\varepsilon_2} & 0 \\ 0 & 0 & \frac{\sigma_3^e}{\varepsilon_3} \end{bmatrix}, \\
D_e^e &= \begin{bmatrix} -1 & 1 & 0 \\ 0 & -1 & 1 \\ 1 & 0 & -1 \end{bmatrix}, M_\varepsilon^e = \begin{bmatrix} \frac{A}{3}\varepsilon_1 & \frac{A}{3}\varepsilon_2 & \frac{A}{3}\varepsilon_3 \end{bmatrix}, F_J^e = \begin{bmatrix} \frac{A}{3} & \frac{A}{3} & \frac{A}{3} \end{bmatrix}, \\
D_h^e &= \begin{bmatrix} \frac{e_{32}\cdot i_x l_1}{2} & \frac{e_{32}\cdot i_y l_1}{2} & \frac{e_{13}\cdot i_x l_2}{2} & \frac{e_{13}\cdot i_y l_2}{2} & \frac{e_{21}\cdot i_x l_3}{2} & \frac{e_{21}\cdot i_y l_3}{2} \end{bmatrix}, \\
M_\mu^e &= \begin{bmatrix} \frac{a_3\cdot i_x l_3}{2}\mu_1 & \frac{a_3\cdot i_y l_3}{2}\mu_1 & \frac{a_3\cdot i_x l_3}{2}\mu_2 & \frac{a_3\cdot i_y l_3}{2}\mu_2 & 0 & 0 \\ 0 & 0 & \frac{a_1\cdot i_x l_1}{2}\mu_2 & \frac{a_1\cdot i_y l_1}{2}\mu_2 & \frac{a_1\cdot i_x l_1}{2}\mu_3 & \frac{a_1\cdot i_y l_1}{2}\mu_3 \\ \frac{a_2\cdot i_x l_2}{2}\mu_1 & \frac{a_2\cdot i_y l_2}{2}\mu_1 & 0 & 0 & \frac{a_2\cdot i_x l_2}{2}\mu_3 & \frac{a_2\cdot i_y l_2}{2}\mu_3 \end{bmatrix}, \\
F_K^e &= \begin{bmatrix} \frac{a_3\cdot i_x l_3}{2} & \frac{a_3\cdot i_y l_3}{2} & \frac{a_3\cdot i_x l_3}{2} & \frac{a_3\cdot i_y l_3}{2} & 0 & 0 \\ 0 & 0 & \frac{a_1\cdot i_x l_1}{2} & \frac{a_1\cdot i_y l_1}{2} & \frac{a_1\cdot i_x l_1}{2} & \frac{a_1\cdot i_y l_1}{2} \\ \frac{a_2\cdot i_x l_2}{2} & \frac{a_2\cdot i_y l_2}{2} & 0 & 0 & \frac{a_2\cdot i_x l_2}{2} & \frac{a_2\cdot i_y l_2}{2} \end{bmatrix}, \\
K^e_{\text{nodal}} &= \begin{bmatrix} 0 & D_e^e \\ -D_h^e & 0 \end{bmatrix}, C^e_{\text{nodal}} = \begin{bmatrix} M_\mu^e & 0 \\ 0 & M_\varepsilon^e \end{bmatrix}, \\
L^e_{\text{nodal}} &= C^e_{\text{nodal}} X^e, F^e_{\text{nodal}} = \begin{bmatrix} F_K^e & 0 \\ 0 & F_J^e \end{bmatrix}, \\
H^e_{\text{nodal}} &= \begin{bmatrix} H_{1x} & H_{1y} & H_{2x} & H_{2y} & H_{3x} & H_{3y} \end{bmatrix}, E^e_{\text{nodal}} = \begin{bmatrix} E_1 & E_2 & E_3 \end{bmatrix}, \\
K^e_{\text{nodal}} &= \begin{bmatrix} K_{1x}^{imp} & K_{1y}^{imp} & K_{2x}^{imp} & K_{2y}^{imp} & K_{3x}^{imp} & K_{3y}^{imp} \end{bmatrix}, J^e_{\text{nodal}} = \begin{bmatrix} J_1^{imp} & J_2^{imp} & J_3^{imp} \end{bmatrix}
\end{aligned}
$$

The matrices with subscript $_{\text{nodal}}$ are the matrices for nodal finite element. Note that X^e is a non-negative diagonal matrix. For edge finite element, the local matrices and the discrete interface condition matrix are defined as follows:

$$
\begin{aligned}
\widehat{D}_e^e &= \begin{bmatrix} -1 & 1 & 0 \\ 0 & -1 & 1 \\ 1 & 0 & -1 \end{bmatrix}, \widehat{M}_\varepsilon^e = \begin{bmatrix} \frac{A}{3}\varepsilon_1 & \frac{A}{3}\varepsilon_2 & \frac{A}{3}\varepsilon_3 \end{bmatrix}, \widehat{F}_J^e = c_4 \begin{bmatrix} \frac{A}{3} & \frac{A}{3} & \frac{A}{3} \end{bmatrix}, \\
\widehat{D}_h^e &= \begin{bmatrix} \frac{l_3}{2} & \frac{-l_2}{2} & \frac{-l_3}{2} & \frac{l_1}{2} & \frac{l_2}{2} & \frac{-l_1}{2} \end{bmatrix}, \\
\widehat{M}_\mu^e &= \begin{bmatrix} \frac{a_2\cdot a_3}{e_{12}\cdot a_2}\frac{l_3}{2}\mu_1 & \frac{a_3\cdot a_3}{e_{13}\cdot a_3}\frac{l_3}{2}\mu_1 & \frac{a_1\cdot a_3}{e_{21}\cdot a_1}\frac{l_3}{2}\mu_2 & \frac{a_3\cdot a_3}{e_{23}\cdot a_3}\frac{l_3}{2}\mu_2 & 0 & 0 \\ 0 & 0 & \frac{a_1\cdot a_1}{e_{21}\cdot a_1}\frac{l_1}{2}\mu_2 & \frac{a_3\cdot a_1}{e_{23}\cdot a_3}\frac{l_1}{2}\mu_2 & \frac{a_1\cdot a_1}{e_{31}\cdot a_1}\frac{l_1}{2}\mu_3 & \frac{a_2\cdot a_1}{e_{32}\cdot a_2}\frac{l_1}{2}\mu_3 \\ \frac{a_2\cdot a_2}{e_{12}\cdot a_2}\frac{l_2}{2}\mu_1 & \frac{a_3\cdot a_2}{e_{13}\cdot a_3}\frac{l_2}{2}\mu_1 & 0 & 0 & \frac{a_1\cdot a_2}{e_{31}\cdot a_1}\frac{l_2}{2}\mu_3 & \frac{a_2\cdot a_2}{e_{32}\cdot a_2}\frac{l_2}{2}\mu_3 \end{bmatrix}, \\
\widehat{F}_K^e &= \begin{bmatrix} \frac{a_2\cdot a_3}{e_{12}\cdot a_2}\frac{l_3}{2} & \frac{a_3\cdot a_3}{e_{13}\cdot a_3}\frac{l_3}{2} & \frac{a_1\cdot a_3}{e_{21}\cdot a_1}\frac{l_3}{2} & \frac{a_3\cdot a_3}{e_{23}\cdot a_3}\frac{l_3}{2} & 0 & 0 \\ 0 & 0 & \frac{a_1\cdot a_1}{e_{21}\cdot a_1}\frac{l_1}{2} & \frac{a_3\cdot a_1}{e_{23}\cdot a_3}\frac{l_1}{2} & \frac{a_1\cdot a_1}{e_{31}\cdot a_1}\frac{l_1}{2} & \frac{a_2\cdot a_1}{e_{32}\cdot a_2}\frac{l_1}{2} \\ \frac{a_2\cdot a_2}{e_{12}\cdot a_2}\frac{l_2}{2} & \frac{a_3\cdot a_2}{e_{13}\cdot a_3}\frac{l_2}{2} & 0 & 0 & \frac{a_1\cdot a_2}{e_{31}\cdot a_1}\frac{l_2}{2} & \frac{a_2\cdot a_2}{e_{32}\cdot a_2}\frac{l_2}{2} \end{bmatrix}, \\
K^e_{\text{edge}} &= \begin{bmatrix} 0 & \widehat{D}_e^e \\ -\widehat{D}_h^e & 0 \end{bmatrix}, C^e_{\text{edge}} = \begin{bmatrix} \widehat{M}_\mu^e & 0 \\ 0 & \widehat{M}_\varepsilon^e \end{bmatrix}, \\
L^e_{\text{edge}} &= C^e_{\text{edge}} X^e, F^e_{\text{edge}} = \begin{bmatrix} \widehat{F}_K^e & 0 \\ 0 & \widehat{F}_J^e \end{bmatrix}, \\
H^e_{\text{edge}} &= \begin{bmatrix} H_{12} & H_{13} & H_{21} & H_{23} & H_{31} & H_{32} \end{bmatrix}, E^e_{\text{edge}} = \begin{bmatrix} E_1 & E_2 & E_3 \end{bmatrix},
\end{aligned}
$$

$$K^e_{\text{edge}} = \left[\begin{array}{cccccc} K^{imp}_{12} & K^{imp}_{13} & K^{imp}_{21} & K^{imp}_{23} & K^{imp}_{31} & K^{imp}_{32} \end{array} \right], J^e_{\text{edge}} = \left[\begin{array}{ccc} J^{imp}_1 & J^{imp}_2 & J^{imp}_3 \end{array} \right].$$

The global matrices C, L, K are assembled from the local matrices by simply stacking the local equations in order (Note that, local numbering of the unknowns is mapped to the global numbering of the unknowns). These global matrices are tall matrices with full column rank.

2) Discrete interfaces conditions: For nodal finite elements, the interfaces continuity is (over-)satisfied, therefore, there is no need for enforcing interface conditions on nodal finite elements. For edge- finite elements, we need to enforce the interface condition $[n \cdot K^{tot}] = 0$ on Γ_i, other interface conditions are satisfied automatically by the field discretization. The interfaces conditions are to be enforced point-wise-ly. Suppose point j and k are on the interface Γ_i, the edge jk is shared by two triangular finite elements $\Delta(i,j,k)$ and $\Delta(j,l,k)$ on both sides of Γ_i as shown in Figure 2. The following equation enforces the interface condition on point j:

$$\begin{aligned} &\mu_j^- \frac{a_i \cdot a_i}{e_{ji} \cdot a_i} H_{ji}(n+1) + \mu_j^- \frac{a_i \cdot a_k}{e_{jk} \cdot a_k} H_{ji}(n+1) + \mu_j^+ \frac{a_l \cdot a_l}{e_{jl} \cdot a_l} H_{jl}(n+1) + \mu_j^+ \frac{a_l \cdot a_k}{e_{jk} \cdot a_k} H_{jk}(n+1) \\ &= \mu_j^- \frac{a_i \cdot a_i}{e_{ji} \cdot a_i} H_{ji}(n) + \mu_j^- \frac{a_i \cdot a_k}{e_{jk} \cdot a_k} H_{ji}(n) + \mu_j^+ \frac{a_l \cdot a_l}{e_{jl} \cdot a_l} H_{jl}(n) + \mu_j^+ \frac{a_l \cdot a_k}{e_{jk} \cdot a_k} H_{jk}(n) \end{aligned} \tag{24}$$

μ_j^- is the permeability in $\Delta(i,j,k)$ and μ_j^+ is the permeability in $\Delta(j,l,k)$. Note that, the enforcing of the point-wise interface condition is not always necessary, because the interfaces conditions are actually enforced in its integral form by the discrete integrated field equations (Add the surface integrated field equations for edge jk in $\Delta(i,j,k)$ and in $\Delta(j,l,k)$, and you will get the corresponding interface condition on edge jk in its integral form). The point-wise interface conditions are enforced to make sure the global system has full column rank and to improve the condition number of the least-squares system. The same kind of equation will be set for point k, the global discrete interfaces conditions $Wu(n+1) = Wu(n)$ is a row-wise collection of these point-wise-ly discrete interface conditions.

F. The least-squares system

After assembling all these global matrices, the set of global over-determined equations to be solved is:

$$\begin{aligned} &(C + \frac{\Delta t}{2} L + \frac{\Delta t}{2} K) u(n+1) = (C - \frac{\Delta t}{2} L - \frac{\Delta t}{2} K) u(n) + \frac{\Delta t}{2} F \frac{f(n+1) + f(n)}{2} \\ &Wu(n+1) = Wu(n) \end{aligned}$$

Where u collects the unknowns and f collects the source terms. After least-squares solution, we have:

$$\begin{aligned} [(C + \frac{\Delta t}{2} L + \frac{\Delta t}{2} K)^H (C + \frac{\Delta t}{2} L + \frac{\Delta t}{2} K) + W^H W] u(n+1) = \\ [(C + \frac{\Delta t}{2} L + \frac{\Delta t}{2} K)^H (C - \frac{\Delta t}{2} L - \frac{\Delta t}{2} K) + W^H W] u(n) \\ + (C + \frac{\Delta t}{2} L + \frac{\Delta t}{2} K)^H F \frac{f(n+1) + f(n)}{2} \end{aligned} \tag{25}$$

In practice, the matrix $(C + \frac{\Delta t}{2} L + \frac{\Delta t}{2} K)^H (C + \frac{\Delta t}{2} L + \frac{\Delta t}{2} K)$ as a whole is assembled from the local matrix $(C^e + \frac{\Delta t}{2} L^e + \frac{\Delta t}{2} K^e)^H (C^e + \frac{\Delta t}{2} L^e + \frac{\Delta t}{2} K^e)$ using the classic matrix assembly procedure of finite element method (so is the righthand side of the linear system); then it is added with $W^H W$ to form the system matrix which is obviously symmetric positive definite. Note that, the matrices L, C, K are never constructed globally in practice; however, they are useful for theoretical analysis.

G. The (weighted) least-squares functional

The least-squares integrated field method can be formulated as finding the minimizer to a weighted Least-squares functional, for which, the exact solution is the minimizer. Let N be the number of finite elements in the computational domain Ω; n be the number of faces in each finite element (two-dimensional triangle elements are extended as prism elements with infinite height. Prism element has 4 faces. $\{S_j, 1 \leq j \leq 4\}$); S_{ij} be the jth face

of the ith element, of which the boundary is defined as ∂S_{ij}; Γ_i be the material interfaces. Over the time interval $\{[t_{k-1}, t_k] : 0 < t_k \leq t, 0 \leq i \leq M, t_k = t_{k-1} + \delta t\}$, we define the least-squares functional in Ω as:

$$\begin{aligned} I &: \mathcal{H}(curl, \Omega) \times \mathcal{H}(curl, \Omega) \rightarrow R, \\ I(E,H) &= \frac{1}{2}\sum_{i=1}^{N}\sum_{j=1}^{n} c_1(ij) \left| \int_{t_k-\delta t}^{t_k} \oint_{\partial S_{ij}} H \cdot dl\, dt - \int_{t_k-\delta t}^{t_k} \int_{S_{ij}} J^{tot} \cdot ds\, dt \right|^2 \\ &+ \frac{1}{2}\sum_{i=1}^{N}\sum_{j=1}^{n} c_2(ij) \left| \int_{t_k-\delta t}^{t_k} \oint_{\partial S_{ij}} E \cdot dl\, dt + \int_{t_k-\delta t}^{t_k} \int_{S_{ij}} K^{tot} \cdot ds\, dt \right|^2 \\ &+ \frac{1}{2}\sum_{i=1}^{N} c_3(ij) \left| \oint_{\cup_{j=1}^{n} S_{ij}} K^{tot} \cdot ds \right|^2 + \frac{1}{2} \sum_{\text{all points on } \Gamma_i} c_4 |[n \cdot K^{tot}]|^2 \end{aligned} \tag{26}$$

where $c_1(ij)$, $c_2(ij)$, $c_3(ij)$ and c_4 are positive weighting factors. We choose the weighting factors such that the coefficients of the equations are of the same magnitude. We may enforce the compatibility equation in the least-squares formulation to eliminate spurious solutions (Note that, the compatibility equation is subsumed in the integrated field equations to all faces of finite elements, therefore, a small or even zero weighting factor can be used). We implement the boundary conditions either implicitly by adding the corresponding squared terms into the least-squares functional or explicitly by restricting the shape functions to satisfy the boundary conditions. We then solve the 2D electromagnetic problem by finding the minimizer to the least-squares functional $I(E, H)$ at each time instance. The sufficient condition for the finite element approximation $E \in \mathcal{H}(curl, \Omega)$ and $H \in \mathcal{H}(curl, \Omega)$ be the minimizer of I is that the variations of I with respect ro E and H equal to 0. Note that: the method we use here is quite similar to the Domain Integrated Field Equation method developed by Peter Jorna et al in [8]. However, due to our assumption that strong inhomogeneity only exists across several material interfaces, the constitutive relations have been used to eliminate the unknown electromagnetic flux. Therefore, the constitutive relations are satisfied exactly and do not participate the least-squares functional minimization procedure. Moreover, the idea, presented by Adrianus T. de Hoop et al in [5], to use node element in homogeneous domain and reserve edge- and face-element expansions for inhomogeneous region comes to reality in this paper. We also want to stress that there have been quite a lot of effort to combine the use of node- and edge- element expansion in literature, see [11], [10], [9], etc. Our method differs from all these methods by utilizing hybrid finite elements to solve time-domain electromagnetic problems based on field integrated equations. We also want to stress that using nodal finite element in homogeneous domain not only save computational time but also model the physics more precisely for the field quantities are continuous in homogeneous (sub-)domain.

H. Consistency

In the system formulation, The equations for boundary conditions are weighted more than other equations, in the numerical solution, they are almost exactly satisfied, therefore, we may consider them as exact equations and eliminate some redundant unknowns in our analysis (which we don't do in practice). For simplicity, we also assume $\sigma^e = 0$, $\sigma^m = 0, \rho = 0$ in the whole computational domain. The Space-time Maxwell's equations can be stated as a constrained initial value problem:

$$\begin{cases} C\dot{u} + Ku = f(t) \\ Wu = 0 \end{cases} \tag{27}$$

where $u = \begin{bmatrix} H & E \end{bmatrix}^T$; $\dot{u}$ is the time derivative of u; The least-squares solution in the trapezoidally discrete time domain is the solution of the linear system:

$$\begin{aligned} &[(C^T + \frac{\Delta t}{2}K^T)(C + \frac{\Delta t}{2}K) + W^T W]u(n+1) \\ -&[(C^T + \frac{\Delta t}{2}K^T)(C - \frac{\Delta t}{2}K) + W^T W]u(n) = (C^T + \frac{\Delta t}{2}K^T)\frac{(f(n+1) + f(n))}{2}\Delta t \end{aligned}$$

A discrete approximation is said to be consistent if it converges to the correct governing equation as the time step size tends to be zero. That is: the residual:

$$\begin{aligned} r(n+1) &= [(C^T+\frac{\Delta t}{2}K^T)(C+\frac{\Delta t}{2}K)+W^TW]u(n+1) \\ &\quad -[(C^T+\frac{\Delta t}{2}K^T)(C-\frac{\Delta t}{2}K)+W^TW]u(n) \\ &- (C^T+\frac{\Delta t}{2}K^T)\frac{(f(n+1)+f(n))}{2}\Delta t \end{aligned}$$

should tend to zero as exact solution is used and time step tends to zero. Moreover, if ϱ is the largest positive integer such that $r_{n+1}=O(\Delta t^{\varrho})$, then the algorithm is said to be of order ϱ. Or equivalently, ϱ is referred to as the order of accuracy or the rate of convergence of the algorithm referring to time step (at this step of analysis, we neglect the space discretization error for simplicity). Expanding $u((n+1)\Delta t)$ and $f((n+1)\Delta t)$ with Taylor series about the time point $n\Delta t$, and using Eq. (27), we obtain:

$$\begin{aligned} r(n+1) &= C^TK\frac{\Delta t^2}{2}\dot{u}(n\Delta t)+\frac{\Delta t^3}{4}K^TK\dot{u}(n\Delta t) \\ &- C^T\frac{\Delta t^2}{4}\dot{f(n)}+O(\Delta t^2)+O(\Delta t^3)+O(\Delta t^4)=O(\Delta t^2) \end{aligned}$$

Assuming the norms of matrices C and K are bounded (which is ensured by correct spacial discretizaton), we have

Theorem 1: The least-squares finite element method with trapezium rule for temporal discretion is of second order accurate in time for the first order partial differential electromagnetic system.

I. The minimum time step

It is well known that a too large time step should be avoided in order to obtain an accurate numerical solution. We shall show that too small time step should be avoided too. At this step of analysis, we shall consider the space discrete error as well. Since we used hybrid linear finite elements to approximate the electromagnetic field strength, the space discrete error is $O(h^2)$; that is:

$$\begin{cases} C\ddot{u}_{exact}+Ku_{exact}-f_{exact}=O(h^2) \\ Wu_{exact}=O(h^2) \end{cases} \tag{28}$$

u_{exact} is the exact solution, $u(n)$ is the finite element approximation. We my write out the total residual as:

$$\begin{aligned} r(n+1) &= [(C^H+\frac{\Delta t}{2}K^H)(C+\frac{\Delta t}{2}K)+W^HW]u(n+1)_{exact} \\ &- [(C^H+\frac{\Delta t}{2}K^H)(C-\frac{\Delta t}{2}K)+W^TW]u(n)_{exact} \\ &- (C^H+\frac{\Delta}{2}K^H)\frac{(f(n+1)_{exact}+f(n)_{exact}+O(h^2))}{2}\Delta t \end{aligned} \tag{29}$$

Expanding the $u(n+1)_{exact}$ and $f(n+1)_{exact}$ with Taylor series about the time point $n\Delta t$ and using Eq.(28), we obtain:

$$\begin{aligned} r(n+1) &= \frac{\Delta t^2}{2}C^HK\dot{u(n)}_{exact}+\frac{\Delta t^3}{4}K^HK\dot{u(n)}_{exact}-\frac{\Delta t^2}{2}C^H\dot{f(n)}_{exact} \\ &+ O(\Delta t^2)+O(h^2)+\Delta tO(h^2)+\Delta t^2O(h^2) \\ &= O(\Delta t^2)+O(h^2)+\Delta tO(h^2) \end{aligned} \tag{30}$$

in which the second order terms dominate, so we only have to study the second order terms $O(\Delta t^2)$ and $O(h^2)$, where $O(h^2)$ only depends on the problem configuration, the mesh and the type of finite elements. After the system is spacial discretized, the $O(h^2)$ term is fixed for every field quantity. It is obvious that, we can decrease Δt to improve the total accuracy until the $O(\Delta t^2)$ is too small and the error term $O(h^2)$, which represents spacial discretization error, dominates the total error; then, further decreasing Δt would not improve the accuracy. In some circumstance, decreasing Δt beyond certain minimum time step would even decrease accuracy, and cost more computation time. For a dedicated analysis on the minimum time step, we refer to [16].

J. The algebraic linear system and iterative solution methods

After the spatial and the temporal dicretization, a linear system of algebraic equations is to be solved. In view of very large system matrices are involved, efficient and fast linear system solver is needed.

1) The linear system: After formulating the linear system, we have the recursive update formula:

$$A_2 u_i = -A_1 u_{i-1} + G_i \tag{31}$$

where u_{i-1} collects the solution of the previous time instance, $u_i = \begin{bmatrix} H_i & E_i \end{bmatrix}^H$ collects the solution of the current time instance. collects the source terms and boundary terms. u_0 collects the initial field strength. Due to the least-squares formulation, A_2 is symmetric positive definite. In fact, one of the main appealing features of the least-squares method is that it always leads to the solution of a symmetric positive definite system.

2) The preconditioned CG-like method: The symmetric positive definite system can be solved with any preconditioned Krylov space iterative solution method. Good preconditioners are needed in iterative solution methods. The preconditioner we used is the incomplete Cholesky factorization (IC). The incomplete Cholesky factorization with dropping threshold 10^{-3} ($IC(10^{-3})$) works very generally and improves iterative convergence a lot. However, direct application of $IC(10^{-3})$ on the matrix A_2 would introduce a lot of fill-ins to the incomplete Cholesky factor. Applying the approximate symmetric minimum degree ordering [2] on the matrix A_2 will reduce the fill-ins of the incomplete Cholesky factor significantly. Then preconditioned Krylov space iterative solvers can be used to solve the symmetric positive definite matrix. The solution method normally takes less than 10 iterations to reach accuracy 10^{-6}. Fewer iterations are needed if the solution of the previous time instance is taken as the initial guess of the current time instance.

VII. Numerical experiments

In this section, our method will be tested with several 2D electromagnetic problems which are difficult to solve for other methods. The computed result will be compared with analytic solutions.

A. Four domain problem

We test our method on a (very rare) example of a situation where at the same time there exists a theoretical solution and the physical set up contains high contrasting regions. The theoretical solution is a 'steady state' solution at a single frequency, containing a source term that continuously injects current. Since we look for a time-domain solution, we use the steady solution at $t = 0$ as initial state, and then start integrating from there in the time domain. Our solution should then follow the actual theoretical steady state solution faithfully. We show that the solution stays stable and the error divergence of our method is much lower than with the classical nodal method using the same coarsely discretized mesh. The configuration is a square domain $\Omega = \{0 \leq x \leq 1, 0 \leq y \leq 1\}$ consisting of four sub-domains $\Omega_i, \{i = 1, 2, 3, 4\}$ with different medium properties (See Table I). Let

$$\begin{aligned} h(t) &= \frac{\sigma^m}{(\sigma^m)^2 + \mu^2\omega^2}\cos(\omega t) + \frac{\mu\omega}{(\sigma^m)^2 + \mu^2\omega^2}\sin(\omega t) \\ g(h) &= \sigma^e \cos(\omega t) - \epsilon\omega \sin(\omega t) \end{aligned}$$

The source density distributions is given by:

$$J_z^{imp} = [-2\pi^2 h(t) - g(t)]\sin(\pi x)\sin(\pi y) \tag{32}$$

$$K_x^{imp} = 0 \tag{33}$$

$$K_y^{imp} = 0 \tag{34}$$

The exact field strengths are:

$$E_z = \sin(\pi x)\sin(\pi y)\cos(\omega t) \tag{35}$$

$$H_x = -\pi h(t)\sin(\pi x)\cos(\pi y) \tag{36}$$

$$H_y = \pi h(t)\cos(\pi x)\sin(\pi y) \tag{37}$$

The angular frequency ω is chosen to be $\pi \times 10^9 rad/s$. The same test configuration in the frequency domain was

TABLE I
CONFIGURATION OF THE FOUR SUB-DOMAINS

Ω_i	Definition of sub-domains	μ_r	σ^m	ϵ_r	σ^e
Ω_1	$0 \leq x < 0.5\ 0 \leq y < 0.5$	1.25	0	1.0	0
Ω_2	$0.5 \leq x \leq 1\ 0 \leq y < 0.5$	2.5	0	1.0	0
Ω_3	$0 \leq x < 0.5\ 0.5 \leq y \leq 1$	1	0	1.0	0
Ω_4	$0.5 \leq x \leq 1\ 0.5 \leq y \leq 1$	1000	0	1.0	0

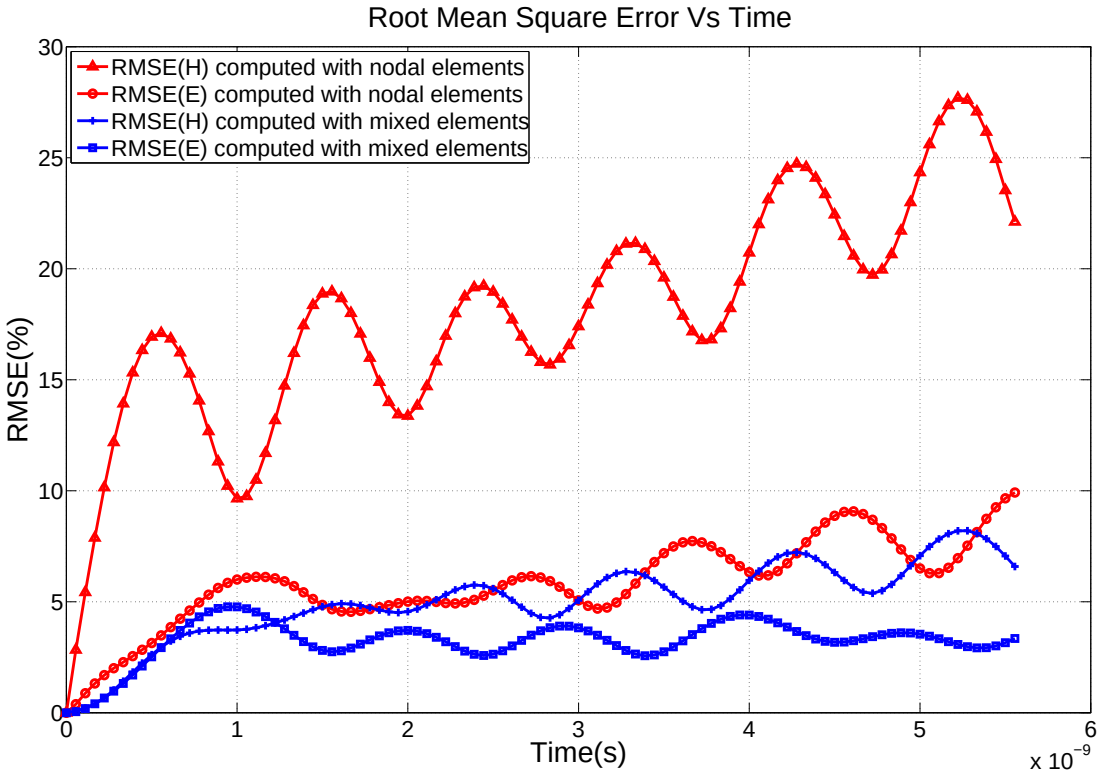

Fig. 6. The root mean square error in the electric field strength (E) and the magnetic field strength (H) in $\Omega \times [0, T]$. 100 time steps have been computed and plotted ($\delta t = 5.5 \times 10^{-11} s$). The RMSE Vs time plot of the electromagnetic field strengths computed with field integrated method based hybrid linear finite elements indicates that the method is accurate and stable.

used by Jorna in [8]. Let the Root Mean Square Error for the field strength F in Ω at time t be:

$$RMSE(F,t) = \left(\frac{\int_\Omega |F(r,t) - F_{exact}(r,t)|^2}{\int_\Omega |\max_{t\in[0,T]} F_{exact}(r,t)|^2}\right)^{\frac{1}{2}} \times 100 \tag{38}$$

With an interface conforming mesh (consists of 289 points and 512 triangular elements) and the exact field strengths at $t = 0$ be the initial value, the $RMSE$s in Ω are plotted in Fig. 6. Note that all $RMSE$s start with 0 at $t = 0$ because the exact solution is taken as the initial value. Experiments have shown that the field strengths computed with mixed elements stay stable and reasonably accurate for this coarse mesh; while the field strengths computed with nodal elements along are unstable and inaccurate. Note that: $\mu_r = 1000$ in Ω_4, since the mesh we used is not fine, any method would produce large numerical errors in Ω_4. However, with our method, the error in Ω_4 does not contaminate the numerical solutions in other regions. One snapshot of the field strength computed with hybrid finite elements is shown in Fig. 7.

B. Homogeneous configuration

We test our method on a time domain example where analytic solution exists. The configuration is a square domain $\Omega = \{0 \leq x \leq 1, 0 \leq y \leq 1\}$ consisting of vaccum ($\epsilon_r = 1, \mu_r = 1, \sigma^e = 0, \sigma^m = 0$). The computational

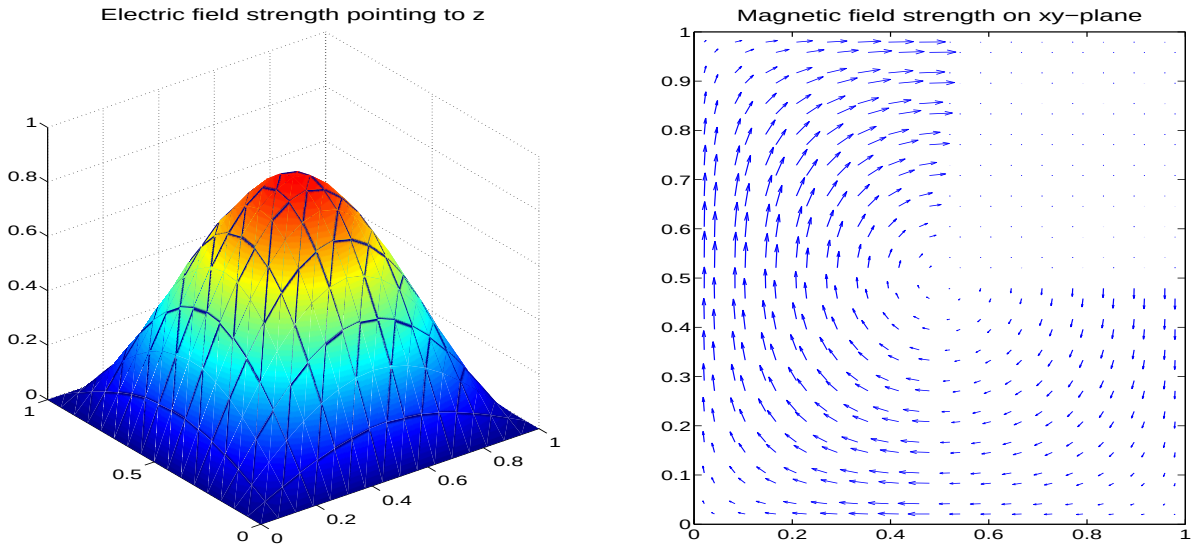

Fig. 7. The snapshot of the electric and magnetic field strengths at $t = 1.667 \times 10^{-10}(s)$ computed with the least-squares field integrated method based on hybrid linear finite elements. The upper right sub-domain is Ω_4 ($\mu_r = 1000$). Errors in Ω_4 do not contaminate the solutions in other regions.

domain is surrounded by PEC boundary. The source densities are given by:

$$J_z^{imp} = A\sin(\omega t)\delta(x-0.5)\delta(y-0.5) \quad (39)$$

$$K_x^{imp} = 0 \quad (40)$$

$$K_y^{imp} = 0 \quad (41)$$

Where $\omega = 2\pi f$, the frequency f is 1GHZ, the wave length $\lambda = c0/f = 0.3m$, $A = 1000$. Assuming the interesting time interval is short enough such that effect of the boundaries does not affect the solution, the analytic solution for electric field strength is known in closed form as:

$$E_z(x,y,t) = \begin{cases} 0, & t < T \\ -\frac{\mu_0}{2\pi}\int_{\tau=T}^{t} \frac{\partial_t J_z^{imp}(t-\tau)}{\sqrt{\tau^2-T^2}} d\tau, & t > T \end{cases} \quad (42)$$

To deal with the singularity at $\tau = T$, let $u = T\cosh(\tau)$, electric field strength can be written as:

$$E_z(x,y,t) = \begin{cases} 0, & t < T \\ -\frac{\mu_0}{2\pi}\int_{u=0}^{\text{acosh}\frac{t}{T}} A\omega\sin(\omega t - \omega T\cosh(u))du, & t > T \end{cases} \quad (43)$$

where $T = \sqrt{(x-0.5)^2+(y-0.5)^2}/c_0$ is the arrival time for the wave to travel from the source location to the observation location. In our finite element approximation, the spacial delta function is approximated with linear finite element approximation. Therefore, the analytic solution will have to be weighted over that domain. We pick the observation point $(x, y) = (0.6, 0.5)$ and compared the computed solution on this point with the analytic solution in the time domain. The solutions computed with different mesh size and time step size are plotted in time domain in Fig.8 Snapshot of the electric field strength are shown in Fig.9. We can see that these simulation solutions agree with the exact solution very well (except the first few time steps). Consequently, we can say we have a good solution, stable for a mesh size close to $\lambda/5$.

C. High conductivity configuration

We test our method on a more realistic example where high contrasts exist. We use zero vector as the initial state, and then start integrating from there in the time domain. The configuration is a square domain $\Omega = \{0 \leq x \leq 1, 0 \leq y \leq 1\}$ consisting of three sub-domains $\Omega_i, \{i = 1, 2, 3\}$ with different medium properties (See Table

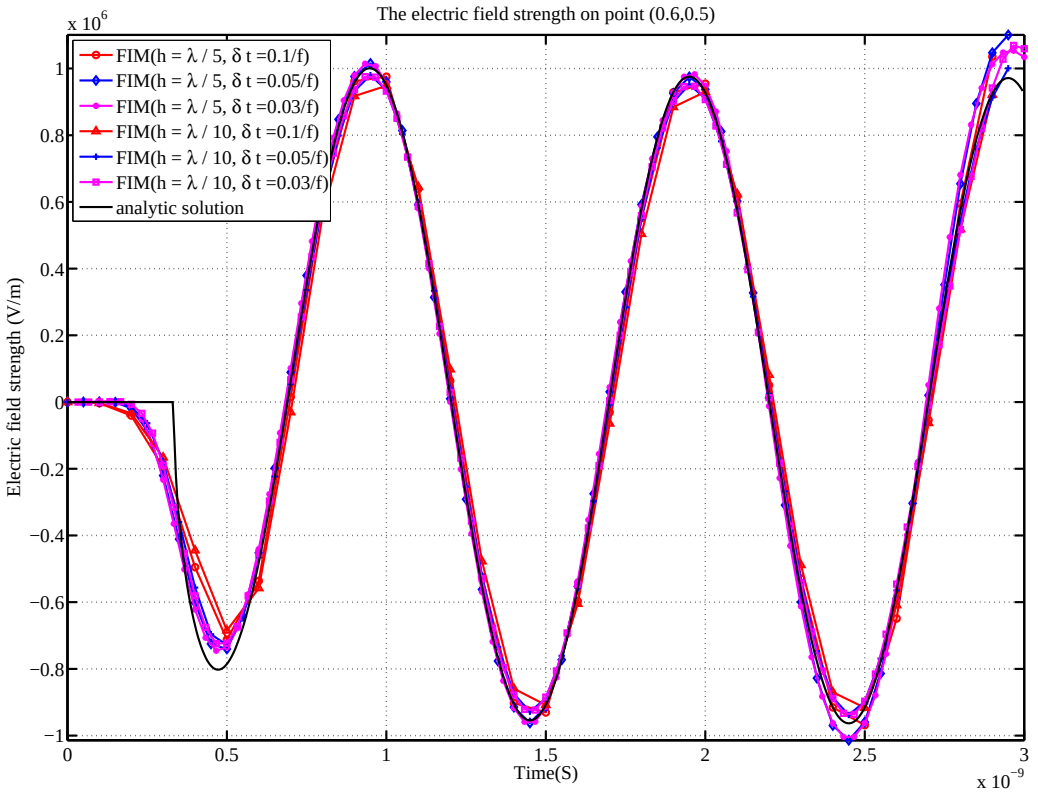

Fig. 8. The electric field strength on observation point $(0.6, 0.5)$ in time domain, analytic solution and the computed solutions with $h_1 = \lambda/5$, $h_2 = \lambda/10$ and $\delta t_1 = \frac{1}{10f} \approx 0.1$ns, $\delta t_2 = \frac{1}{20f} \approx 0.05$ns, $\delta t_3 = \frac{1}{30f} \approx 0.033$ns. The analytic solution is weighted over the discrete 2D delta function.

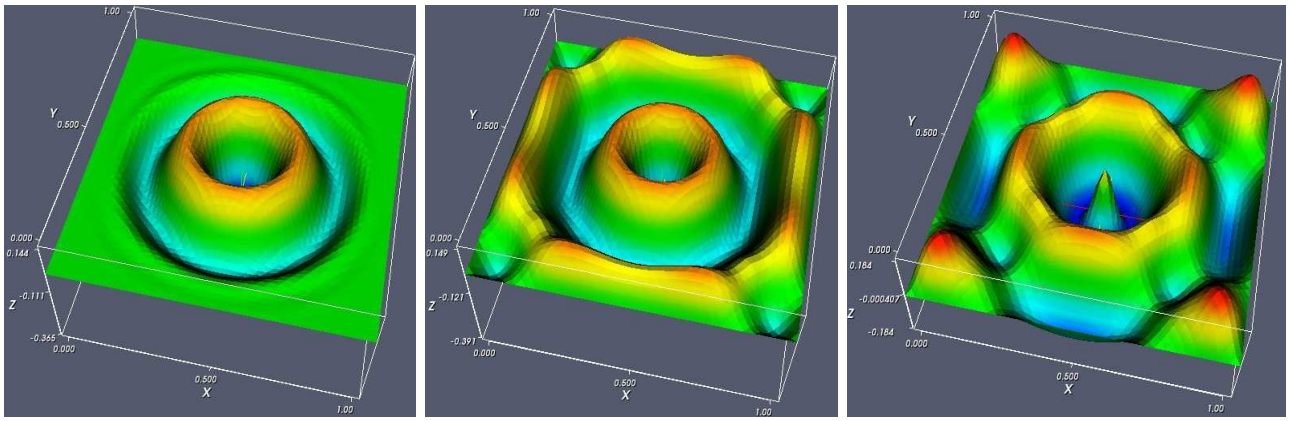

Fig. 9. The snapshots of the electric field strengths at $t_1 = 1.23$ns, $t_2 = 2.17$ns, $t_3 = 2.47$ns computed with the least-squares field integrated method.

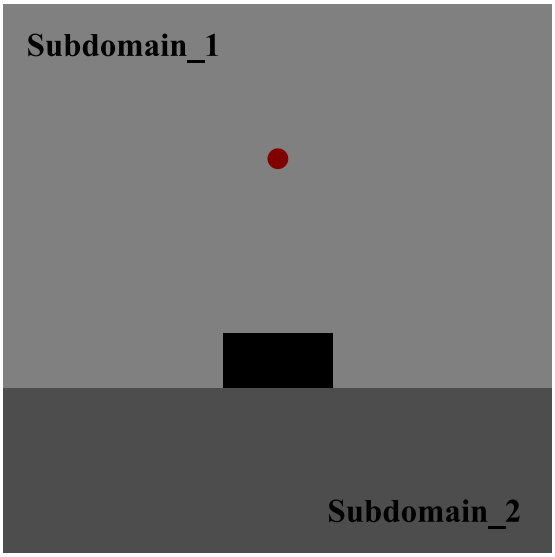

Fig. 10. The configuration of the third experiment

TABLE II
CONFIGURATION OF THE THIRD EXPERIMENT

Ω_i	Definition of sub-domains	μ_r	σ^m	ϵ_r	σ^e
Ω_1	$0 \leq x < 1\ 0 \leq y < 0.3$	1	0	2	0
Ω_2	$0.4 \leq x \leq 0.6\ 0.3 \leq y < 0.4$	1	0	1	10^7
Ω_3	$\Omega - \Omega_1 - \Omega_2$	1	0	1	0

II and Fig. 10). The computational domain is surrounded by PEC boundary. The source densities are given by:

$$J_z^{imp} = -\chi(t)\sqrt{2\theta e}(t-t_0)\exp[-\theta(t-t_0)^2]\delta(x-0.5)\delta(y-0.5) \quad (44)$$

$$K_x^{imp} = 0 \quad (45)$$

$$K_y^{imp} = 0 \quad (46)$$

Where $\chi(t)$ is the heaviside step function, the peak frequency f_{peak} is 1GHZ, $t_0 = 2$ns, $\theta = 2\pi^2 f_{\text{peak}}^2$. the simulation is done in time domain. As always, edge- finite elements are used on interfaces only, nodal finite elements are used elsewhere. Snapshots of electric field strength computed with hybrid finite elements are shown in Fig. 11.

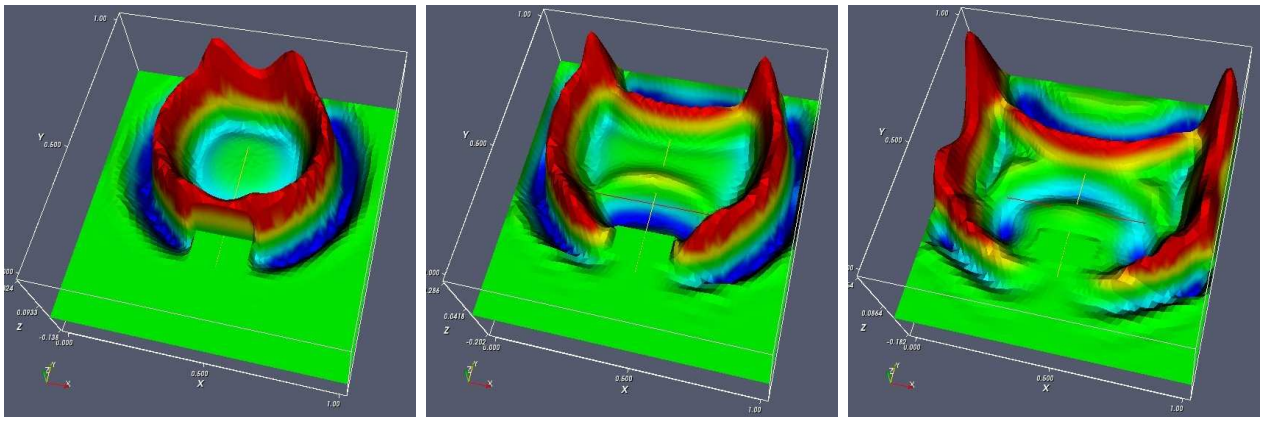

Fig. 11. The snapshot of electric field strength at $t_1 = 3$ns,$t_2 = 3.3$ns, $t_3 = 3.7$ns computed with $h = \lambda/10$, $\delta t = 0.033$ns

VIII. Time domain analysis with Uniaxial Perfectly Matched Layers

For electromagnetic wave computation, it is important to be able to model the unbounded problems where the computational domain extends to infinity. In this paper, we adopt the analysis and perfected matched layers discussed by A. T. de hoop et al in [1].

A. Theory

Let's now first review the second order wave equation for electric field strength (assuming not lossless media and smooth changing isotropic, time-invariant, instantly reacting medium):

$$\nabla \times \nabla \times E + c^{-2}\partial_t^2 E = Q^i \tag{47}$$

where Q^i summarizes all source terms (electric current and magnetic current). Knowing that:

$$\nabla \times \nabla \times E = \nabla(\nabla \cdot E) - \nabla^2 E \tag{48}$$

Assuming that no charges presents in the domain, we have $\nabla \cdot E = 0$ and the second order Maxwell's equation is equivalent to the following wave equation:

$$\nabla^2 E - c^{-2}\partial_t^2 E = -Q^i \tag{49}$$

Assuming the computational domain $D \cup \partial D$ is embedded by infinite source free domain D^∞, That is:

$$\nabla^2 E - c^{-2}\partial_t^2 E = 0, \text{ in } D^\infty \tag{50}$$

$$Q^i \subset D \tag{51}$$

The electric field in the computational domain can be computed analytically using the Green's function:

$$E(r,t) = \int_D G(r,r',t) *^{(t)} [Q^i(r',t) + Q^s(r',t)]dV(r') \tag{52}$$

in which

$$G(r,r',t) = \frac{\delta(t-R/c)}{4\pi R},\ R = \|r-r'\| \tag{53}$$

where $r = [x,y,z]$ and the origin point is defined inside D, $\|v\|$ computes the 2-norm of vector v. The time domain solution can be transformed into frequency domain by Laplace transformation. Then solution:

$$\widehat{E}(r,s) = \int_D \widehat{G}(r,r',s)[\widehat{Q}^i(r',s) + \widehat{Q}^s(r',s)]dV(r') \tag{54}$$

in which

$$\widehat{G}(r,r',s) = \frac{\exp(-sR/c)}{4\pi R},\ R = \|r-r'\| \tag{55}$$

solves the equation:

$$\nabla^2 E - c^{-2}\partial_t^2 E = -Q^i \tag{56}$$

Knowing that, the objective is to construct a solution in domain $D \cup D_{pml}$ which equals $\widehat{E}(r,s)$ in $D \cup \partial D$ and takes whatever value in domain D_{pml}. Coordinate stretching can do the job, let:

$$\widehat{X} = \int_0^x \chi_x(\xi,s)d\xi,\ \widehat{Y} = \int_0^y \chi_y(\xi,s)d\xi,\ \widehat{Z} = \int_0^z \chi_z(\xi,s)d\xi \tag{57}$$

$$\partial_{\widehat{X}} = \chi_x(x,s)^{-1}\partial_x,\ \partial_{\widehat{Y}} = \chi_y(x,s)^{-1}\partial_y,\ \partial_{\widehat{Z}} = \chi_z(x,s)^{-1}\partial_z \tag{58}$$

construct χ_x, χ_y and χ_z such that $\chi_x = \chi_y = \chi_z = 1$ in domain D. Let $\widehat{r} = [\widehat{X},\widehat{Y},\widehat{Z}]$, $\widehat{r} = r$ in domain D; the Green's function:

$$\widetilde{G}(\widehat{r},\widehat{r}',s) = \frac{\exp(-s\widehat{R}/c)}{4\pi\widehat{R}},\ \widehat{R} = \|\widehat{r}-\widehat{r}'\| \tag{59}$$

would equal to $\widehat{G}(r,r',s)$ in domain $D\cup\partial D$.

$$\widetilde{E}(\widehat{r},s)=\int_D \widetilde{G}(\widehat{r},\widehat{r}',s)[\widehat{Q}^i(\widehat{r}',s)+\widehat{Q}^s(\widehat{r}',s)]dV(r') \tag{60}$$

shall solve the equation:

$$\widehat{\nabla}^2\widetilde{E}-c^{-2}s^2\widetilde{E}=-\widehat{Q}^i \text{ where } \widehat{\nabla}^2=\partial^2_{\widehat{X}}+\partial^2_{\widehat{Y}}+\partial^2_{\widehat{Z}} \tag{61}$$

which is equivalent to the un-stretched wave equation in domain D. Then we need to choose $\chi_x(\xi,s)$, $\chi_y(\xi,s)$, $\chi_z(\xi,s)$ such that $\widetilde{E}(\widehat{r},s)$ is attenuated or delayed in D^{pml}, such that the outgoing EM wave never comes back to the computational domain. So long as the wave in Perfectly Matched Layers D^{pml} are heavily attenuated or delayed, coordinate stretching can be performed without changing the electromagnetic waves in the computational domain $D\cup\partial D$.

B. Implementation of UPML in 2D problems

In this section, we are going to derive the 2D UPML for Maxwell's equations by stretching the coordinate. The resulted PML is equivalent to Perfectly Matched Uniaxial Medium by Sacks et al [17]. Let's first review the 2D(TM) Maxwell's equations in frequency domain (for simplicity, we omit sources and conductivity):

$$\begin{aligned}\partial_x H_y-\partial_y H_x &= s\varepsilon E_z &(62)\\ \partial_y E_z &= -s\mu H_x &(63)\\ \partial_x E_z &= s\mu H_y &(64)\end{aligned}$$

Stretch the coordinate as:

$$\begin{aligned}\widehat{X} &= \int_0^x \chi_x(\xi,s)d\xi &(65)\\ \widehat{Y} &= \int_0^y \chi_y(\xi,s)d\xi &(66)\\ & &(67)\end{aligned}$$

Then

$$\begin{aligned}\partial_{\widehat{X}} &= \chi_x(x,s)^{-1}\partial_x &(68)\\ \partial_{\widehat{Y}} &= \chi_y(x,s)^{-1}\partial_y &(69)\\ & &(70)\end{aligned}$$

Replace the original coordinate with the stretched ones, we get:

$$\begin{aligned}\chi_x(x,s)^{-1}\partial_x\widehat{H}_y-\chi_y(y,s)^{-1}\partial_y\widehat{H}_x &= s\varepsilon\widehat{E}_z &(71)\\ \chi_x(y,s)^{-1}\partial_y\widehat{E}_z &= -s\mu\widehat{H}_x &(72)\\ \chi_x(x,s)^{-1}\partial_x\widehat{E}_z &= s\mu\widehat{H}_y &(73)\end{aligned}$$

$\widehat{H}$ and $\widehat{E}$ be the field strength on the stretched coordinate. Say $\widetilde{H}_x=\chi_x(x,s)\widehat{H}_x$, $\widetilde{H}_y=\chi_y(y,s)\widehat{H}_y$, note that they are still equal to the original field in the computational domain. Then we have:

$$\begin{aligned}\partial_x\widetilde{H}_y-\partial_y\widetilde{H}_x &= s\varepsilon\chi_x(x,s)\chi_y(y,s)\widehat{E}_z &(74)\\ \partial_y\widehat{E}_z &= -s\mu\chi_x(x,s)^{-1}\chi_y(y,s)\widetilde{H}_x &(75)\\ \partial_x\widehat{E}_z &= s\mu\chi_x(x,s)\chi_y(y,s)^{-1}\widetilde{H}_y &(76)\end{aligned}$$

Direct transformation from frequency domain to time domain would result in convolution in time domain. To avoiding this, We introduce more unknowns:

$$\begin{aligned}\widetilde{B}_x &= \chi_x(x,s)^{-1}\chi_y(y,s)\mu\widetilde{H}_x &(77)\\ \widetilde{B}_y &= \chi_x(x,s)\chi_y(y,s)^{-1}\mu\widetilde{H}_y &(78)\\ \widehat{D}_z &= \varepsilon\chi_y(y,s)\widehat{E}_z &(79)\end{aligned}$$

therefore the original equations become:

$$\begin{aligned}
\partial_x \widetilde{H}_y - \partial_y \widetilde{H}_x &= s\chi_x(x,s)\widehat{D}_z && (80)\\
\partial_y \widehat{E}_z &= -s\widetilde{B}_x && (81)\\
\partial_x \widehat{E}_z &= s\widetilde{B}_y && (82)\\
\widetilde{B}_x &= \chi_x(x,s)^{-1}\chi_y(y,s)\mu\widetilde{H}_x && (83)\\
\widetilde{B}_y &= \chi_x(x,s)\chi_y(y,s)^{-1}\mu\widetilde{H}_y && (84)\\
\widehat{D}_z &= \varepsilon\chi_y(y,s)\widehat{E}_z && (85)
\end{aligned}$$

Let $\chi_x(x,s) = 1 + \frac{\sigma_x}{s\varepsilon_0}$, $\chi_y(y,s) = 1 + \frac{\sigma_y}{s\varepsilon_0}$ which introduce attenuation in the Perfectly Matched Layers, and transform the equations form frequency domain to the time domain:

$$\begin{aligned}
\partial_x \widetilde{H}_y - \partial_y \widetilde{H}_x &= (\partial_t + \sigma_x/\varepsilon_0)\widehat{D}_z && (86)\\
\partial_y \widehat{E}_z &= -\partial_t \widetilde{B}_x && (87)\\
\partial_x \widehat{E}_z &= \partial_t \widetilde{B}_y && (88)\\
(\varepsilon_0\partial_t + \sigma_x)\widetilde{B}_x &= \mu(\varepsilon_0\partial_t + \sigma_y)\widetilde{H}_x && (89)\\
(\varepsilon_0\partial_t + \sigma_y)\widetilde{B}_y &= \mu(\varepsilon_0\partial_t + \sigma_x)\widetilde{H}_y && (90)\\
\partial_t \widehat{D}_z &= \varepsilon(\partial_t + \sigma_y/\varepsilon_0)\widehat{E}_z && (91)
\end{aligned}$$

Trapezoidal discretization in time domain would need all four types of unknowns (H, B, E, D). Applying leap-frog schema in time greatly reduces the number of unknowns. And we discretize space with discrete field integrated equations, B and H locate on half time level, while D and E locate on whole time level, then we have the successive update formula as follows:

$$\begin{aligned}
\int_S B(n+3/2) &= -\Delta t \oint_{\partial S} E(n+1)dl \\
&+ \int_S B(n+1/2) - \Delta t \int_S K(n+1)ds && (92)\\
H_x(n+3/2) &= \frac{2\varepsilon_0 - \sigma_y\Delta t}{2\varepsilon_0 + \sigma_y\Delta t}H_x(n+1/2) \\
+\frac{1}{\mu(2\varepsilon_0 + \sigma_y\Delta t)}&[(2\varepsilon_0 + \sigma_x\Delta t)B_x(n+3/2) - (2\varepsilon_0 - \sigma_x\Delta t)B_x(n+1/2)] && (93)\\
H_y(n+3/2) &= \frac{2\varepsilon_0 - \sigma_x\Delta t}{2\varepsilon_0 + \sigma_x\Delta t}H_y(n+1/2) \\
+\frac{1}{\mu(2\varepsilon_0 + \sigma_x\Delta t)}&[(2\varepsilon_0 + \sigma_y\Delta t)B_y(n+3/2) - (2\varepsilon_0 - \sigma_y\Delta t)B_y(n+1/2)] && (94)\\
\int_S [1 + \frac{\sigma_x\Delta t}{2\varepsilon}]D_z(n+2)ds &= \Delta t \oint_{\partial S} H(n+3/2)dl \\
&+ \int_S [1 - \frac{\sigma_x\Delta t}{2\varepsilon_0}]D_z(n+1)ds - \int_S J_z(n+3/2)ds && (95)\\
E_z(n+2) &= \frac{2\varepsilon - \Delta t\sigma_y}{2\varepsilon_0 + \Delta t\sigma_y}E_z(n+1) \\
&+\frac{1}{(2\varepsilon_0 + \Delta t\sigma_y)\varepsilon}[2\varepsilon_0 D_z(n+2) - 2\varepsilon_0 D_z(n+1)] && (96)
\end{aligned}$$

spacial discretization are done with combined edge- nodal- finite elements. Note that for this schema, divergence free condition need to be applied explicitly, or the method will be unconditionally unstable. Also, after the leap-frog schema is conditionally stable but second order accurate. The chosen sampling frequency must be less than one-half of the highest resonant frequency of the mesh (see [15]). σ_x and σ_y are PML parameters that control the absorption ratio. Never too large nor too small should it be. To avoid spurious reflections, it should be increased smoothly from 0 on the boundary of computational domain and to σ_{max} on the outer boundary of PML layer where PEC or

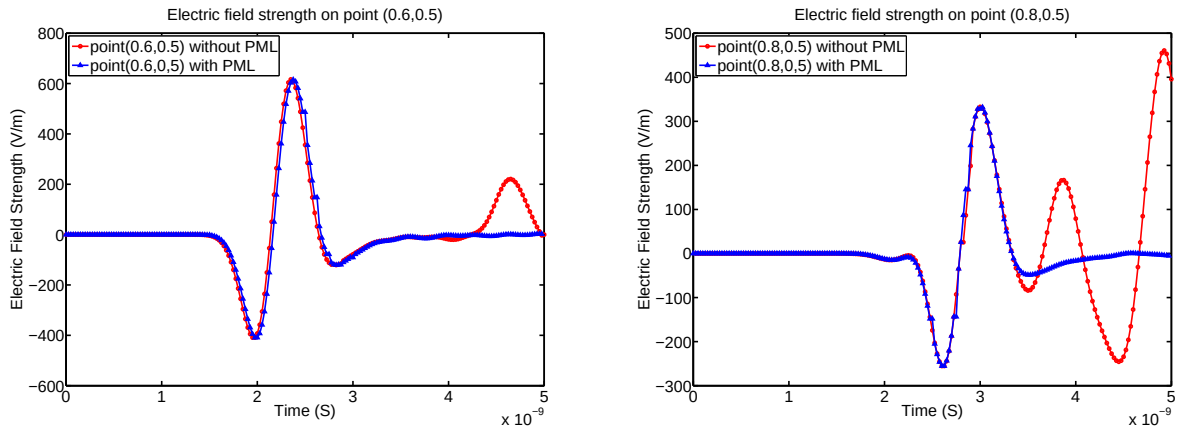

Fig. 12. The electric field strength on observation point $(0.6, 0.5)$ and $(0.8, 0.5)$ in the time domain computated on a mesh consisting 545 points. When needed, the Perfectly Matched Layers presents in $D^{PML} = \{0 \leq x \leq 0.1 \cup 0.9 \leq x \leq 1, 0 \leq y \leq 0.1 \cup 0.9 \leq y \leq 1\}$ which is of three elements thick. The maximum $\sigma_{max} = 0.4257$, which is computed with Eq. 97. The optimum configuration of the UPML is out of the scope of this paper, please refer to [14] for more details .

PMC can be used to truncate the whole domain. Third order or fourth order polynomials is normally used, σ_{max} can be chosen heuristically according to the following formula:

$$\sigma_{opt} = -\frac{(m+1)\ln[R(0)]}{2\eta d} \tag{97}$$

where m is the order of the polynomial used; $R(0)$, the reflection ratio of normal incident wave; d, the thickness of the PML layer; $\eta = \sqrt{\mu/\varepsilon}$, the impedance. See [14] for more details. With all field quantities normalized as shown in section VI-B, χ should be nomralized as: $\hat{\chi} = 1 + \hat{\sigma}$ and $\hat{\sigma} = \sigma L\sqrt{\mu_0/\varepsilon_0}$

C. Numerical experiments with UPML

We test our method with uniaxial Perfectly Matched Layers on a time domain example where analytic solution exists. The configuration is a square domain $\Omega = \{0.1 \leq x \leq 0.9, 0.1 \leq y \leq 0.9\}$ consisting of vaccum ($\epsilon_r = 1, \mu_r = 1, \sigma^e = 0, \sigma^m = 0$). The computational domain is surrounded by PMLs $D^{PML} = \{0 \leq x \leq 0.1 \cup 0.9 \leq x \leq 1, 0 \leq y \leq 0.1 \cup 0.9 \leq y \leq 1\}$. The PML loss profile is graded smoothly from 0 to $\sigma_{max} = 0.4257$ by third order polynomials. The source densities are given by:

$$J_z^{imp} = -\chi(t)\sqrt{2\theta e}(t - t_0)\exp[-\theta(t - t_0)^2]\delta(x - 0.5)\delta(y - 0.5) \tag{98}$$

$$K_x^{imp} = 0 \tag{99}$$

$$K_y^{imp} = 0 \tag{100}$$

Where $\chi(t)$ is the heaviside step function, the peak frequency f_{peak} is 1GHZ, $t_0 = 2$ns, $\theta = 2\pi^2 f_{\text{peak}}^2$. We pick the observation points $(0.6, 0.5)$ and $(0.8, 0.5)$ and choose the observation time interval long enough such that reflection (if any) can be well observed. The solutions computed with and without PMLs are plotted in time domain in Fig.12.

IX. Conclusion

The least-squares field integrated method based on hybrid linear finite elements holds considerable promise to model electromagnetic effects in integrated circuits, where high contrasts between different types of materials is the rule and complex structures are present.

X. Acknowledgements

The authors gratefully acknowledge the support from from the Marie Curie Fellowship program and the support from the Technology Foundation STW under the MICES project. The authors hereby acknowledge the fact that Prof. A.T. de Hoop provided the central idea (the use of edge elements) of the paper and gratefully thank him for his contributions to the MICES project. The author also would like to thank Prof. Daniel IOAN at Numerical Methods Laboratory in "Politehnica" University of Bucharest for the useful discussions.

REFERENCES

[1] Robert F. Remis Adrianus T. de Hoop and Peter M. van den Berg. The 3d wave equation and its cartesian coordinatestretched perfectly matched embedding c a time-domain greens function performance analysis. *Journal of Computational Physics*, 221:88–105, 2007.

[2] P. Amestoy, T. A. Davis, and I. S. Duff. Amd, an approximate minimum degree ordering algorithm. *ACM Transactions on Mathematical Software*, 30:381–388, Sept 2004.

[3] F. Assous, P. Degond, and J. Segre. Numerical approximation of the maxwell equations in inhomogeneous media by a p^1 conforming finite element method. *Journal of computaional physics*, 128(0217), Feb 1996.

[4] Rickard Bergstrom and Mats G. larson. Discontiuous least-squares finite element methods for the div-curl problem. *SIAM rev.*, 40:789–837, 1998.

[5] Adrianus T. de Hoop and Ioan E. Lager. Static magnetic field computation - an approach based on the domain-integrated field equations. *IEEE TRANSACTIONS ON MAGNETICS*, 34(5), 1998.

[6] Mur G. and de Hoop A.T. A finite-element method for computing three-dimensional electromagnetic fields in inhomogeneous media. *Magnetics, IEEE Transactions on*, 21:2188–2191, Nov 1985.

[7] BO-NAN Jiang. *The Least-Squares Finite Element Method: Theory and Applications in Computational Fluid Dynamics and Electromagnetics (Scientific Computation)*. 2006.

[8] Pieter Jorna. Integrated field equations methods for the computation of electromagnetic fields in strongly inhomogeneous media. *PhD thesis, TUDelft*, Feb 2005.

[9] I. E. Lager. *Finite element modelling of static and stationary electric and magnetic fields*. PhD thesis, Delft University of Technology, 1996.

[10] Ioan E. Lager and Gerrit Mur. Generalized cartesian finite elements. *IEEE TRANSACTIONS ON MAGNETICS*, 34(4):2220–2227, july 1998.

[11] Gerrit Mur. The finite-element modeling of three-dimensional electromagnetic fields using edge and nodal elements. *IEEE tranactions on antennas and propagation*, 41(7), July 1993.

[12] Barba P.D., Perugia I., and Savini A. Recent experiences on mixed finite elements for 2d simulations of magnetic fields. *COMPEL: Int J for Computation and Maths. in Electrical and Electronic Eng.*, 17(5), 1998.

[13] J. Schoberl. Netgen - an advancing front 2d/3d-mesh generator based on abstract rules. *Comput.Visual.Sci*, 1:41–52, 1997.

[14] Allen Taflove and Susan C. Hagness. *Computational Electrodynamics: The Finite-Difference Time-Domain Method*, volume Chapter 7, Perfectly Matched Layers Absorbing Boundary Conditions. Artech House Publishers; 2nd edition, 2000.

[15] Daniel Arthur White. *Discrete Time Vector Finite Element Methods for Solving Maxwell's Equations on 3D unstructured Grids*, pages 77–78. Phd thesis, 1997.

[16] Chaodong Yang and Yongan Gu. Minimum time-step criteria for galerkin finite element methods applied to one-dimensional parabolic paratial differential equations. *Wiley InterScience*, June 2005.

[17] Sacks Z.S., D.M. Kingsland, Lee R., and Jin-Fa Lee. A perfectly matched anisotropic absorber for use as an absorbingboundary condition. *Antennas and Propagation, IEEE Transactions on*, 43(12):1460–1463, Dec 1995.